Journal of Materials Chemistry

Cite this: J. Mater. Chem., 2012, 22, 13956

www.rsc.org/materials

PAPER

A functional triazine framework based on *N*-heterocyclic building blocks†

Stephan Hug,[ab] Michael E. Tauchert,[b] Shen Li,[b] Ursula E. Pachmayr[b] and Bettina V. Lotsch*[ab]

Received 28th February 2012, Accepted 10th May 2012
DOI: 10.1039/c2jm31248d

Covalent organic frameworks constitute a subclass of polymeric materials offering enhanced porosity, functionality and stability. In this work a covalent triazine framework based on bipyridine building blocks is presented, along with a comprehensive elucidation of its local structure, porosity, and capacity for metal uptake. A typical synthesis was carried out under ionothermal conditions at 400 700 °C using $ZnCl_2$ as a Lewis acidic trimerization catalyst. A high degree of local order and the presence of triazine and bipyridine moieties are ascertained at a synthesis temperature of 400 °C, along with micropores and specific surface areas of up to 1100 $m^2 g^{-1}$. Mesopores are increasingly formed at synthesis temperatures above 450 °C, yielding highly porous frameworks with hierarchical porosity and exceptionally large surface areas in excess of 3200 $m^2 g^{-1}$ at 700 °C. We demonstrate the capability of the bipyridine unit to provide specific and strong binding sites for a large variety of transition metal ions, including Co, Ni, Pt and Pd. The degree of metal loading (up to 38 wt%) can be tuned by the metal concentration in solution and is dependent on both the type of metal as well as the temperature at which the CTF was synthesized. Evidence for site specific metal coordination bodes well for the use of metal loaded CTFs as heterogeneous catalysts carrying homogeneous type active sites.

1. Introduction

The rational design of porous solids from molecular building blocks as seen in the rise of metal organic framework (MOF) chemistry has pushed the borders of porous materials from inorganic oxidic materials into the realm of supramolecular and polymer chemistry.[1–3] Assembling well defined organic building blocks into regular, porous arrays enables a unique combination of local, molecular properties embedded within a supramolecular matrix whose properties are governed by the interaction and mutual arrangement of the molecular building blocks, as well as the overall periodic structure and morphology of the bulk material.

The development of new representatives of MOFs has lately been driven by the quest for rationally designed framework topologies with inherent and well dispersed functional groups. Whereas a range of textbook examples of MOFs with exceptionally high porosities and specific surface areas has been prepared to date, the design of MOFs featuring functional organic linkers tailor made for specific applications has been hampered by the requirement of unconventional synthetic approaches combined with low framework stability and loss of porosity upon framework modification.

In general, framework stability may be greatly enhanced by replacing the metal clusters or ions connecting the organic ligands in MOFs by another set of organic linkers, thereby substituting potentially reactive electrostatic bonds between the building blocks by strong, covalent bonds, which are less prone to hydrolysis and thermal degradation. The resulting, all organic class of porous solids, dubbed porous cross linked polymers (PCPs)[4–7] or porous organic polymers (POPs),[8–10] is devoid of structurally active metal ions and entirely constructed of light weight, rigid and covalently linked organic building blocks. Covalent organic frameworks (COFs) constitute a subclass of POPs, often featuring long range order similar to their metal organic counterparts. The prototypical COF topologies created initially by Yaghi, Lavigne and others[1,11–13] are composed of boronic acid building blocks forming ester linkages with poly alcohols or boroxine rings by self condensation under relatively mild conditions. Recently, Antonietti, Thomas and co workers pioneered COF chemistry by introducing a new generation of COFs based on triazine linkages, termed covalent triazine frameworks (CTFs).[2,14] CTFs are prepared by trimerization of the cyano groups of aromatic nitriles *via* ionothermal synthesis in a Lewis acidic medium, typically in $ZnCl_2$ salt melts. Except for a few examples,[2,15] CTFs oftentimes lack long range order, yet excel by their high porosities paired with exceptional chemical

[a]*Max Planck Institute for Solid State Research, Heisenbergstr. 1, 70569 Stuttgart, Germany. E mail: b.lotsch@fkf.mpg.de; Fax: +49 711 689 1612; Tel: +49 711 689 1611*
[b]*Department of Chemistry, University of Munich (LMU), Butenandtstr. 5 13, 81377 Munich, Germany. E mail: bettina.lotsch@cup.uni muenchen. de; Fax: +49 89 2180 77440; Tel: +49 89 2180 77429*

† Electronic supplementary information (ESI) available: Tables of used materials, temperature programs, elemental analysis and metal doping. Details of used methods, sorption measurements, DTA/TG and XRD of sample 5, EA and IR of samples 13 16, DTA/TG and IR of DCBPY, SEM/EDX of a Pt loaded sample, and the ^{15}N solid state NMR spectrum of CTF 1. See DOI: 10.1039/c2jm31248d

inertness and high thermal stability owing to their graphite like composition and robust carbon carbon and carbon nitrogen linkages. The presence of stoichiometric and well defined nitrogen sites in the triazine frameworks has recently been shown to render CTFs promising catalysts and catalyst supports,[16 18] as catalytically active metal ions may be site selectively anchored to the CTF matrix by strong nitrogen metal interactions in large amounts owing to the large accessible surface area. Moreover, the metal ions can be reduced *in situ* or the CTF may be impregnated with already formed metal nanoparticles, yielding hybrid materials with well dispersed nanoparticles immobilized on the CTF support. Apparently, N doping has a beneficial influence on the dispersion efficiency and binding of the surface anchored nanoparticles to the porous support, as seen for instance in N doped carbon nanotubes or N doped activated carbons as compared to their unmodified counterparts.[19 22] Likewise, metal modified CTF catalysts exhibit superior activity, stability and, hence, recyclability in oxidation reactions as compared to other carbon supports modified with smaller amounts of nitrogen.[16,17]

In order to provide a larger amount of possibly more Lewis basic binding sites compared to triazine rings, a heteroaromatic CTF building block featuring well defined N sites capable of strong binding to various metal ions would be desirable. Along these lines, Kuhn *et al.* recently introduced *o* dicyanopyridine as a CTF building block featuring a higher amount of nitrogen than the prototypic dicyanobenzene linker.[2,14] As expected by the higher nitrogen content, the resulting Pt modified framework showed high activity and superior stability compared to the homogeneously catalyzed Periana type selective oxidation of methane to methanol featuring a 2,2′ dipyrimidine as a ligand.[18,23] In this system, however, no detailed information on the local structure of the catalyst and type of metal binding was accessible owing to the poor long range order of the CTF scaffold.

With these design principles in mind, we targeted a CTF based on the 5,5′ dicyano 2,2′ bipyridine (DCBPY) building block, where the bipyridine (*bipy*) unit acts as a scaffold to site specif ically coordinate the metal cations. Owing to the abundance of metal *bipy* complexes known and the versatility of the *bipy* ligand in homogeneous catalysis, a CTF framework based on this ubiquitous type of ligand may ultimately provide a link between a homogeneous catalyst and its heterogeneous counterpart, both featuring a metal *bipy* unit as the catalytically active site. First attempts to synthesize a *bipy* CTF have been made by Kuhn *et al.* recently,[14] yet the resulting amorphous powders were reported to possess no apparent porosity and a surface area of essentially zero. In the present paper we demonstrate the synthesis of a highly porous *bipy* CTF and give a detailed account of the complex interplay between local and long range order, porosity, and nitrogen content to enable a deeper under standing of the structure and a more rational approach to the design of covalent triazine frameworks.

2. Experimental

2.1. Materials

All reactions were carried out under an argon atmosphere in flame dried glassware. Anhydrous solvents and liquid reagents were transferred using a syringe or a cannula. Unless otherwise noted, all materials were obtained from commercial suppliers (see ESI, Table S1†) and used without further purification. Column chromatography was performed using silica gel (0.035 0.070 mm, 60 Å, Acros Organics). Tetrakis (triphenylphosphine) palladium[24] and tri(2 furyl)phosphine (tfp)[25] were synthesized according to published procedures. THF was continuously refluxed and freshly distilled from sodium benzophenone ketyl under nitrogen. Detailed information about the methods used is available in the ESI†.

2.2. Precursor synthesis

(5-Bromopyridin-2-yl)zinc(II) chloride. In a Schlenk tube LiCl (2.79 g, 66.0 mmol) and Mg turnings (1.82 g, 75.0 mmol) were suspended in THF (6.75 mL). 1,2 Dibromoethane (0.14 mL, 1.50 mmol) and chlorotrimethylsilane (200 μL, 1.50 mmol) were added and the suspension heated shortly to reflux. The reaction was cooled to 25 °C and a solution of $ZnCl_2$ in THF (0.65 M, 51.0 mL, 33.0 mmol) and, subsequently, 5 bromo 2 iodopyridine (8.52 g, 30.0 mmol) in THF (20.3 mL) was added. The mixture was stirred for 6 h at 25 °C and left overnight to precipitate metal residues. The resulting solution was used without any further purification. The concentration of (5 bromopyridin 2 yl)zinc(II) chloride was determined by iodolysis[26] (0.37 M, 97%).

5,5′-Dibromo-2,2′-bipyridine.[27] (5 Bromopyridin 2 yl)zinc(II) chloride (0.37 M in THF, 54.0 mL, 20.0 mmol), $Pd(dba)_2$ (287 mg, 0.50 mmol), and tri(2 furyl)phosphine (232 mg, 1.00 mmol) were mixed in a Schlenk flask. 5 Bromo 2 iodopyridine (4.73 g, 16.7 mmol) in THF (11.5 mL) was slowly added and the mixture was stirred for 1 h at 50 °C. The reaction was quenched by the addition of a saturated aqueous solution of NH_4Cl (150 mL) and the resulting mixture was extracted with $CHCl_3$ (5 × 150 mL). The combined organic layers were washed with brine (200 mL), dried over $MgSO_4$ and concentrated *in vacuo*. The crude product (4.73 g) was purified by flash column chromatography (CH_2Cl_2/*n* hexane 1 : 1) yielding 5,5′ dibromo 2,2′ bipyridine as colorless crystals (1.30 g, 4.14 mmol, 25%). ^{1}H NMR (270 MHz; $CDCl_3$): δ 8.70 (2H, d, $^4J_{HH} = 2$ Hz, $C^{5/5'}H$), 8.29 (2H, d, $^3J_{HH} = 9$ Hz, $C^{2/2'}H$), 7.93 (2H, dd, $^3J_{HH} = 9$ Hz, $^4J_{HH} = 2$ Hz, $C^{3/3'}H$); $^{13}C\{^1H\}$ NMR (68 MHz; $CDCl_3$): δ 153.6 ($C^{1/1'}$), 150.3 ($C^{5/5'}$), 139.8 ($C^{3/3'}$), 122.4 ($C^{2/2'}$), 121.6 ($C^{4/4'}$).

5,5′-Dicyano-2,2′-bipyridine.[28] A microwave vial was charged with degassed DMF (20.0 mL), 5,5′ dibromo 2,2′ bipyridine (1.25 g, 4.00 mmol), $Zn(CN)_2$ (0.94 g, 8.00 mmol), $Pd(PPh_3)_4$ (0.28 g, 0.24 mmol), and bis(diphenylphosphino)pentane (0.11 g, 0.24 mmol). A stream of argon was then bubbled through the mixture for 2 min and the vial was sealed. The yellow mixture was heated in the microwave for 5 min at 150 °C. The now turquoise suspension was poured into H_2O (300 mL) and $CHCl_3$ (300 mL) and was stirred for 1 h. The solvent layers were sepa rated and the water layer extracted with $CHCl_3$ (3 × 300 mL). The combined organic layers were dried over $MgSO_4$ and concentrated *in vacuo*. The crude product was purified by flash column chromatography (CH_2Cl_2 ethyl acetate 9 : 1) to give 5,5′ dicyano 2,2′ bipyridine as colorless crystals (0.76 g, 3.69 mmol, 92%). ^{1}H NMR (400 MHz; $CDCl_3$): δ 8.96 (2H, d,

$^{4}J_{HH}$ = 2 Hz, $C^{5/5'}H$), 8.63 (2H, dd, $^{3}J_{HH}$ = 8 Hz, $^{5}J_{HH}$ = 1 Hz, $C^{2/2'}H$), 8.13 (2H, dd, $^{3}J_{HH}$ = 8 Hz, $^{4}J_{HH}$ = 2 Hz, $C^{3/3'}H$); $^{13}C\{^{1}H\}$ NMR (100 MHz; $CDCl_3$): δ 157.0 ($C^{1/1'}$), 152.2 ($C^{5/5'}$), 140.6 ($C^{3/3'}$), 121.8 ($C^{2/2'}$), 116.6 ($C^{4/4'}$), 110.8 ($C^{6/6'}$).

2.3. Synthesis of covalent triazine frameworks

In a typical synthesis a *Duran* or quartz ampoule (1 × 14 cm) was charged with 5,5′ dicyano 2,2′ bipyridine (100 mg, 480 μmol) and $ZnCl_2$ (332 mg, 2.40 mmol) within a glove box. The ampoule was flame sealed under vacuum and was subjected in a tube oven to the temperature programs outlined in Table S2†. After cooling to ambient temperature, the ampoule was opened and its content was ground thoroughly. The crude product was stirred in H_2O (150 mL) for 3 h, filtered, and washed with H_2O (150 mL) and acetone (75 mL). The mixture was then refluxed in 1 M HCl (150 mL) overnight, filtered, and subsequently washed with 1 M HCl (3 × 75 mL), H_2O (15 × 75 mL), THF (3 × 75 mL), and acetone (3 × 75 mL). Finally, the product was dried under vacuum for 6 h at 300 °C.

2.4. Metal doping experiments

In a typical experiment the CTF (10 mg, 0.05 mmol) was sus pended in a solution of the desired metal salt (500 mol% with respect to the 2,2′ bipyridine building block) in 10 mL of water and stirred overnight at 60 °C. The doped CTF was filtered, washed with H_2O (50 mL) and acetone (15 mL), and dried overnight at 90 °C.

3. Results and discussion

3.1. Synthesis and porosity

The synthesis of DCBPY was carried out starting from 5 bromo 2 iodopyridine in a three step microwave assisted process as outlined in the Experimental section.

A standard CTF synthesis was performed under ionothermal conditions in sealed glass ampoules at 400 °C for 48 h using a $ZnCl_2$ salt melt both as a solvent and a Lewis acidic trimeri zation catalyst (Scheme 1). As opposed to typical COF syntheses, which are usually carried out in high boiling solvents, the salt melt approach has turned out to be beneficial in CTF systems with respect to ensuring chemical equilibrium and, hence, reversibility by keeping the as formed oligomers and polymers solvated throughout the polymerization process and preventing them from phase separating and precipitating irreversibly.[2,14] In accordance with previous studies, the monomer to salt ratio as well as the reaction temperature both have a strong impact on the degree of framework order (local and long range) and porosity of the resulting material.[14,29] As outlined in Table 1 (entries 1 8), a DCBPY : $ZnCl_2$ ratio of 1 : 5 yielded samples with the highest porosities, whereas higher salt contents led to slightly lower porosities, and one equivalent of $ZnCl_2$ to none. The order of the material did not show any significant dependency on the salt concentration, in contrast to observations made by Kuhn *et al.*[14] In order to probe the influence of temperature on the chemical composition and structure of the obtained materials, the reaction temperatures were varied between 375 and 700 °C. Although materials with drastically different surface areas (SA) between

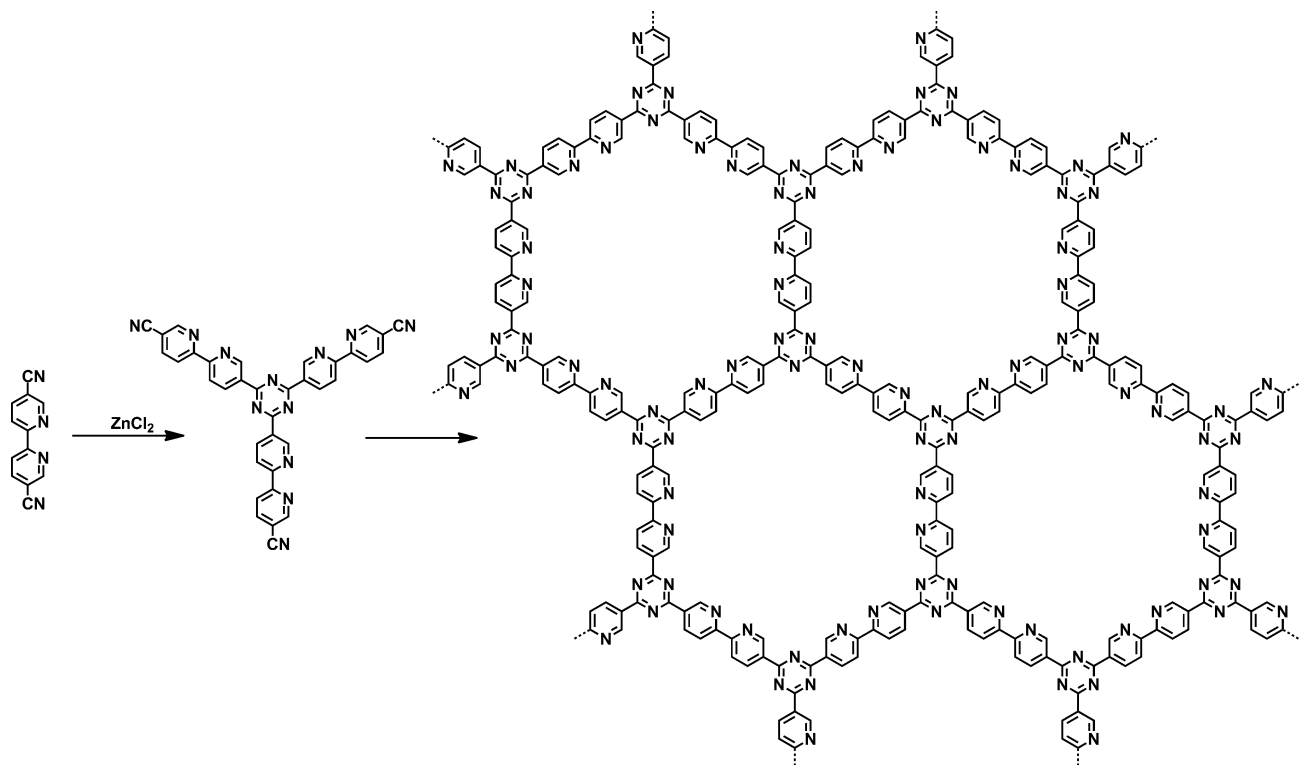

Scheme 1 Schematic illustration of the synthesis of *bipy* CTF. The bifunctional DCBPY trimerizes to an extended network under ionothermal conditions.

Table 1 Overview of the reaction conditions and porosity properties of different *bipy* CTF materials

Sample	Temp [°C]	Time [h]	$ZnCl_2$ [mol equiv.]	S_{BET} [m^2 g^{-1}]	Total pore vol.[a] [cm^3 g^{-1}]
1	375	48	1		
2	375	48	5	928	0.46
3	375	48	7.5	876	0.43
4	375	48	10	800	0.40
5	400	48	5	671	0.37
6	400	48	5	1108	0.58
7	400	48	7.5	1108	0.58
8	400	48	10	964	0.49
9	450	48	5	945	0.46
10	500	48	5	1432	0.68
11	600	48	5	2393	1.19
12	700	48	5	3219	1.66
13	400/600	40/0.2	5	1663	0.81
14	400/600	40/20	5	2187	1.10
15	400/600	40/40	5	2761	1.44
16	400/600	40/80	5	2509	1.22

[a] At P/P_0 0.99.

~670 and 3220 m^2 g^{-1} were obtained, the standard synthesis temperature was adjusted to 400 °C to maximize porosity and at the same time prevent partial framework decomposition. The impact of temperature on porosity will be discussed in more detail in Section 3.3.

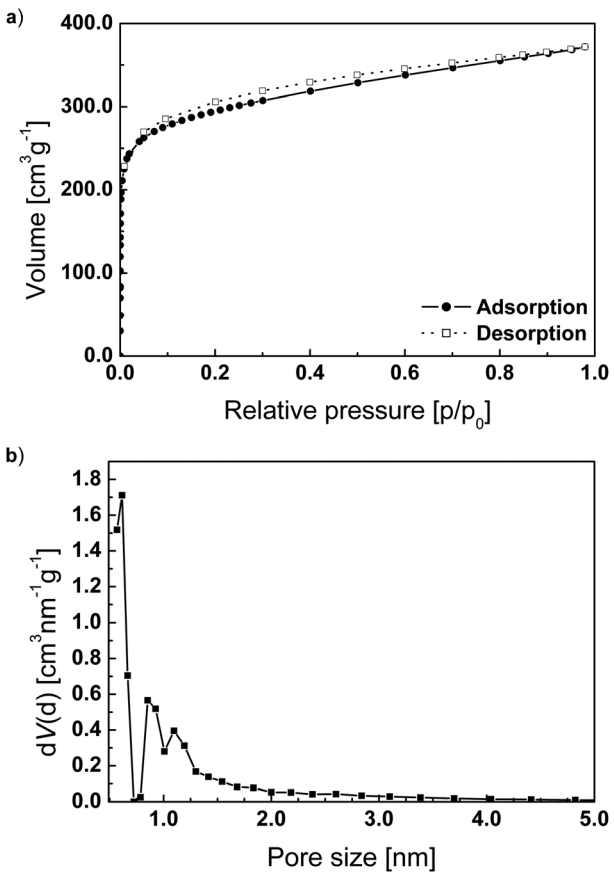

Fig. 1 (a) N_2 physisorption isotherm of *bipy* CTF 400. (b) Pore size distribution of *bipy* CTF 400.

The adsorption isotherm and pore size distribution of a sample obtained at 400 °C (*bipy* CTF 400) are shown in Fig. 1. The sorption behavior is indicative of a highly microporous material with a large fraction of ultramicropores with sizes just below 6 Å and a smaller fraction of micropores with diameters around 1 nm. Interestingly, we found significant variations in the porosity for different samples (SA 671 1108 m^2 g^{-1}; tot. pore vol. 0.36 0.58 cm^3 g^{-1}) despite using the same reaction conditions (Table 1, entries 5 and 6) and chemical composition. This observation can be rationalized by the fact that even slight variations in the synthesis conditions (heating rate, temperature inhomogeneities, *etc.*) shift the pore size distribution towards slightly smaller ultramicropores with sizes just below 5 Å, which are not accessible anymore to nitrogen used as a probe molecule in the physisorption measurements (see ESI, Fig. S1†). Consequently, the apparent total surface area is noticeably reduced if the fraction of ultramicropores with pore sizes below the N_2 accessibility threshold is increased.

3.2. Local structure

With applications ranging from sensing to heterogeneous catalysis with homogeneous (*i.e.* molecular) reaction sites, the versatility and functionality of a CTF are largely governed besides its porosity by its local structure. This is especially true for CTFs carrying functional groups such as the *bipy* unit, which needs to withstand the harsh ionothermal synthesis conditions described above. To the best of our knowledge, little is known yet about the local structure of CTF materials, irrespective of the building blocks used, as most porous CTFs prepared so far show little or no crystallinity, even at the local scale. In order to probe the structural properties of the *bipy* CTF 400 and ascertain the influence of the synthesis conditions on the *bipy* group, the *bipy* CTF 400 was studied by X ray powder diffraction (XRD), FTIR and solid state NMR spectroscopy.

As known from other CTFs except CTF 1 and a non porous naphthalene CTF,[2,15] *bipy* CTF 400 was found to be largely amorphous, except for broad peaks around ~13 and 25° 2θ, the latter of which we attribute to the 00*l* reflection indicating a "graphitic" layer stacking with an interlayer distance of ~3.6 Å (Fig. S2†). Contrary to its X ray amorphous character which indicates a lack of long range order of the polymeric network, the IR spectrum exhibits a number of well resolved, sharp bands suggesting a high degree of order on the local scale (Fig. 2).

Notably, the strong bands at 1506 (in plane deformation vibration of the triazine ring) and 822 cm^{-1} (out of plane deformation vibration), as well as the absence of nitrile bands at 2364 and 2336 cm^{-1} compared to the starting material indicate the formation of triazine rings.[30,31] The doublet band around 1550 1600 cm^{-1}, as well as the less well resolved bands between 1000 and 1450 cm^{-1} and the sharp band at 740 cm^{-1} may be largely attributed to the C=N and ring stretching vibrations of the *bipy* moiety.[32] For comparison, the IR spectrum of the model compound 2,4,6 tri(pyridin 2 yl) 1,3,5 triazine (TPT) is shown in Fig. 2 (top). This molecular compound features building blocks (triazine, pyridine) similar to those expected to be present in the *bipy* CTF 400. The bands of the TPT spectrum mostly correspond well to those of the *bipy* CTF 400, showing triazine bands at 1522 and 815 cm^{-1} and a doublet around 1580 1600 cm^{-1}, as

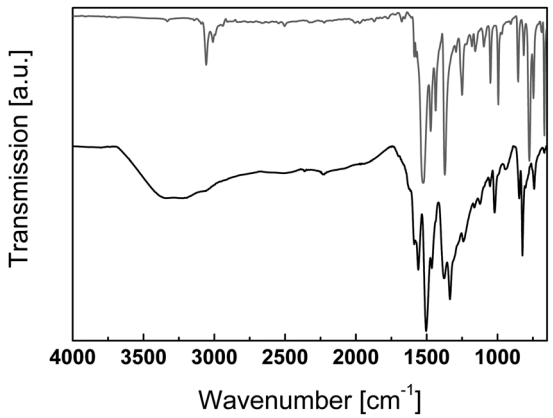

Fig. 2 IR spectrum of *bipy* CTF 400 (black) and TPT.

well as two strong bands at 775 and 745 cm ^{1} which we ascribe to pyridine ring vibrations.[32]

For further information on the local structure we performed ^{13}C and ^{15}N MAS solid state NMR measurements and compared the former to the ^{13}C spectrum of TPT. As depicted in Fig. 3, the ^{13}C spectrum of *bipy* CTF 400 shows six well resolved signals at 170 (1), 157 (2), 149 (3), 134 (4), 130 (5), and 119 ppm (6). The peak positions nicely correspond to those of TPT, which shows an essentially identical pattern, except for a single, broadened signal around 151 ppm (2 3) instead of two well resolved signals in the *bipy* CTF 400 at 149 (3) and 157 ppm (2) owing to the different substitution patterns. The peak at 170 ppm (1) can unambiguously be assigned to the triazine ring carbon atoms.[33] Likewise, the assignment of the peak pattern of the *bipy* part is well established and consistent with an increasing downfield shift of the carbon atoms located in *meta* , *para* , and *ortho* position to the nitrogen atoms in the two rings, respectively. Our proposed overall assignment scheme is given in Fig. 3a (bottom). Although the pyridine moiety adjacent to the triazine ring in the model compound has a different substitution pattern compared to that in the *bipy* CTF 400, the NMR spectra are essentially insensitive to this difference in the local connection scheme.

The intact local structure is additionally confirmed by the ^{15}N NMR spectrum of the *bipy* CTF 400 (Fig. 3b). The signal at 128 ppm can be assigned to the triazine moiety (compare CTF 1 in Fig. S3†) and likewise, the signal at 70 ppm is char acteristic of the bipyridine unit.[34] Note that in addition to the well defined building blocks present in the material after synthesis, the *bipy* CTF 400 is highly stable in concentrated acids and bases such as H_2SO_4 and KOH for several hours without showing any sign of degradation.

3.3. Thermal behavior: porosity tuning

As noted by Kuhn *et al.* the synthesis conditions such as temperature, heating rate, salt precursor ratio, *etc.* greatly impact the structural properties of the obtained materials.[14,29] Notably, we detected a strong correlation between the SA and the porosity of our materials and the temperature at which they were synthesized, thus furnishing a dynamic system that is highly tunable in terms of porosity. Whereas samples obtained at 400 °C show SA between 600 and 1100 m^2 g ^{1} (see above), samples synthesized at temperatures between 450 and 700 °C (Table 1, entries 9 12) exhibit drastically increased SA with up to 3219 m^2 g ^{1} for *bipy* CTF 700 (Fig. 4). On a microscopic level, this significant increase in SA is the consequence of a gradual widening of the pores, accompanied by a shift of the pore size distribution toward the mesopore range without affecting the micropores (Fig. 5). While for *bipy* CTF 400 a bimodal pore size distribution at 5 and 10 Å is observed and essentially no meso pores are present, the sizes of both the ultramicropores and micropores slightly widen and small mesopores are increasingly formed above 500 °C. Although micropores are present at all

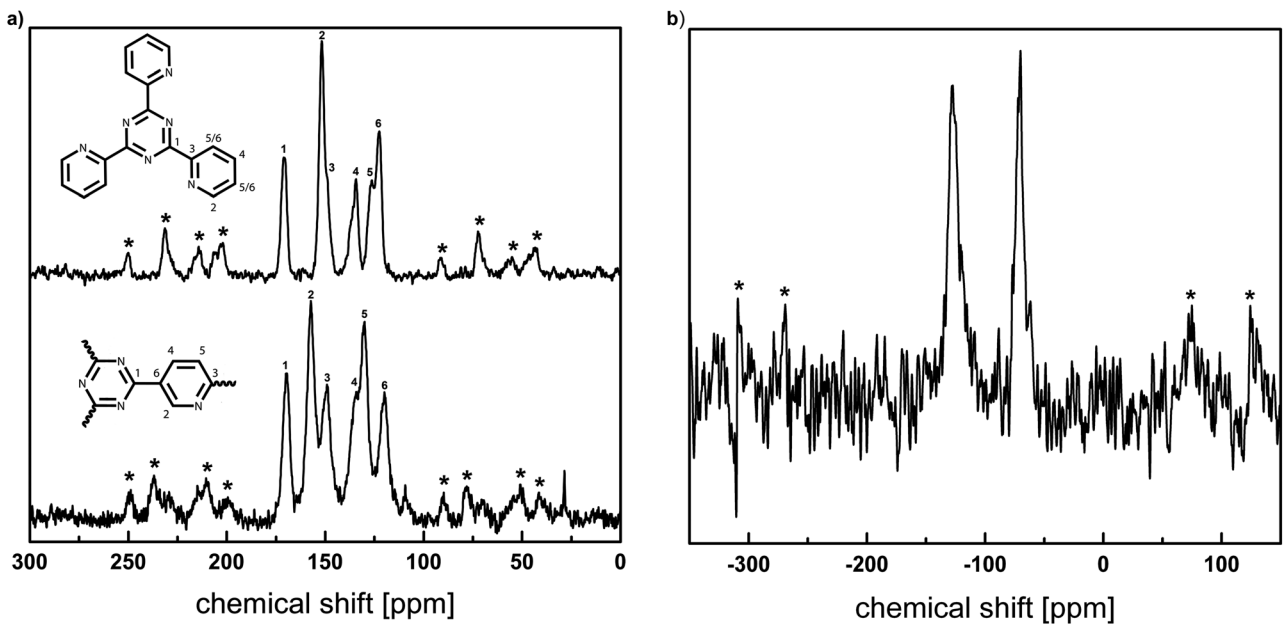

Fig. 3 (a) ^{13}C solid state MAS NMR spectrum of *bipy* CTF 400 (bottom) compared to the model compound TPT (top). (b) ^{15}N ssNMR spectrum of *bipy* CTF 400.

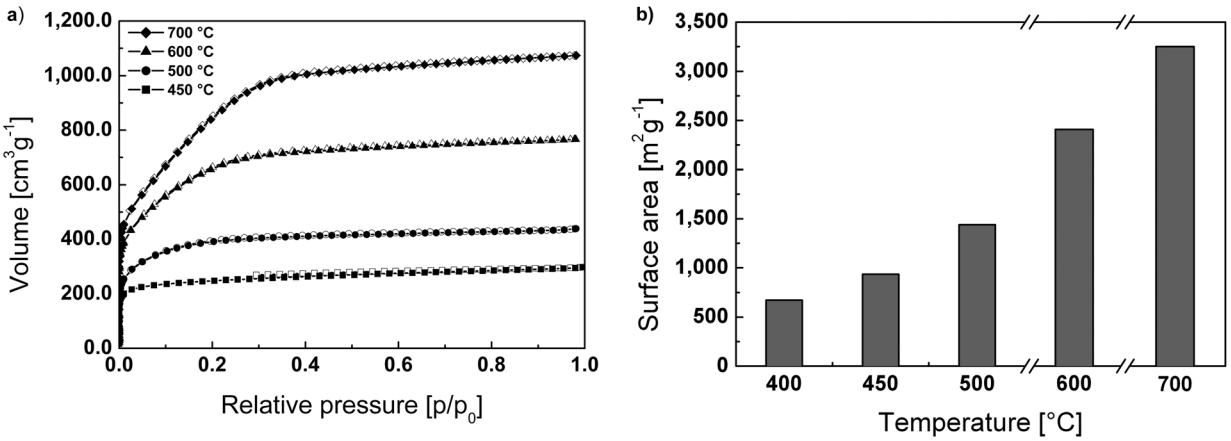

Fig. 4 (a) N_2 physisorption isotherms of samples synthesized at 450 700 °C. (b) Surface areas of samples synthesized at 400 700 °C.

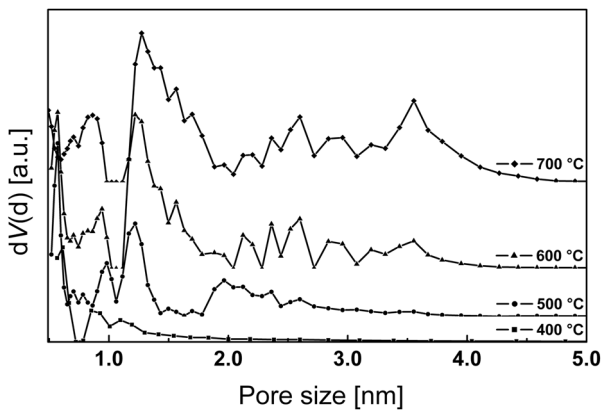

Fig. 5 Comparison of the pore size distributions of samples synthesized at 400 700 °C.

temperatures, the volume fraction of mesopores with pore diameters between 2 and 4 nm is dominant for *bipy* CTF 700.

In order to correlate the porosity changes with the compo sition and structure of the materials, the compounds obtained at different temperatures were studied by elemental analysis (EA) and IR and NMR spectroscopy. As can be seen from the DTA/TG of *bipy* CTF 400, thermal degradation commences around 450 °C and becomes quite rapid above 500 °C (Fig. S4†). Whereas about 10% of weight is lost below 150 °C due to adsorbed water or solvents occluded in the pores, the weight loss due to framework degradation amounts to ~20 23% at 700 °C and ~46% at 1000 °C. EA conclusively indicates a gradual nitrogen loss at temperatures higher than 400 °C, accompanied by an equally pronounced loss of hydrogen and a slight increase in the relative carbon content, thereby indi cating progressive carbonization of the materials (Table S3†, entries 5 and 9 12 and Fig. 6a). If the weight loss associated with framework degradation observed in the TG is assumed to be exclusively due to nitrogen, at 700 °C approximately 80% of nitrogen is gone, whereas at 600 °C a loss of only about 26% nitrogen is observed. Similarly, by extrapolation we expect a loss of ~50% nitrogen at about 650 °C, which corresponds to either all bipyridine or all triazine nitrogens. Chemically, the compositional changes were monitored most conclusively by IR and NMR spectroscopy (Fig. 6b and 7). Notably, the triazine signature is lost already at a temperature as low as 500 °C, indicated by the absence of the triazine ring breathing mode around 820 cm ^{1} and the increasingly featureless fingerprint region in the IR, as well as by the complete loss of the triazine signal at 170 ppm in the ^{13}C NMR in a sample treated at 400 and 600 °C for 40 h each.

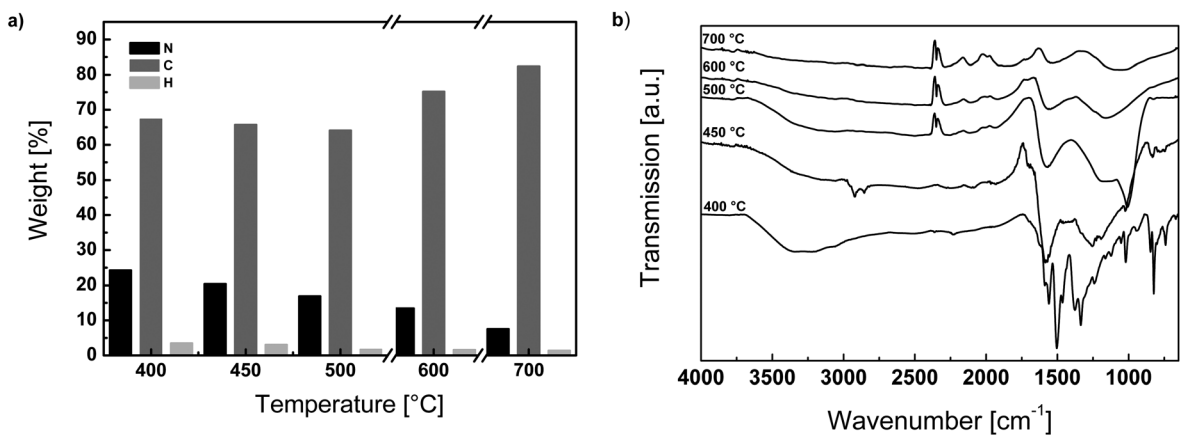

Fig. 6 (a) Variation of carbon (gray), hydrogen (light gray) and nitrogen (black) contents as a function of the synthesis temperature of *bipy* CTF. (b) IR spectra of *bipy* CTFs subjected to different temperature programs.

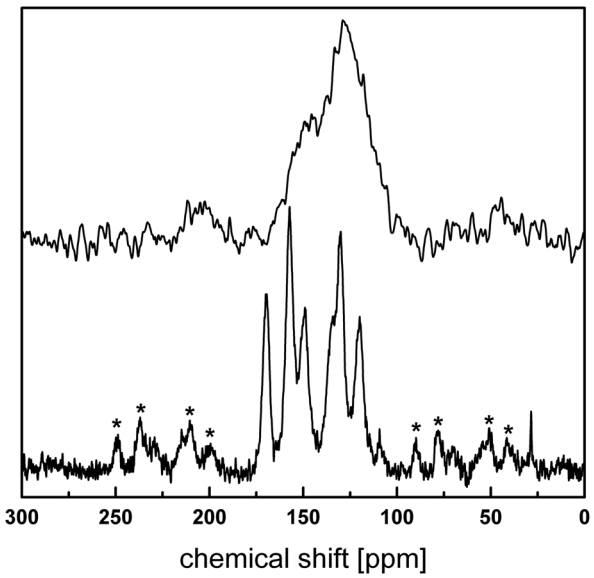

Fig. 7 ^{13}C solid state MAS NMR spectrum of *bipy* CTF 400 (bottom) compared with sample 15 obtained at 600 °C (top).

Also, the low field ^{13}C signals of the bipyridine unit lose intensity relative to those at higher field, indicating the delayed, yet gradual loss of nitrogen from the bipyridine ring starting at temperatures around 600 °C. Note, however, that the degradation temperatures cannot directly be compared to those obtained from DTA/TG, as the temperature program and especially the holding times significantly varied compared to the *ex situ* studies. We conclude that the initial and rapid loss of nitrogen can be attributed almost exclusively to the degradation of triazine rings, which is then followed by decomposition of the bipyridine rings and carbonization at higher temperatures. A likely degradation mechanism is the thermally induced retro trimerization of the triazine rings and subsequent rearrangements, giving rise to loss of N_2 and possibly irreversible formation of new C C bonds. The former may lead to "foaming" of the network and the latter to cross linking between the layers, both resulting in the observed local expansion of the network and the drastic enhancement of porosity and SA.

Insights into the kinetics of the thermal degradation were obtained by heating a sample synthesized at 400 °C to 600 °C for increasing periods of time. Even at only 12 minutes at 600 °C, noticeable framework amorphization and significantly reduced triazine ring vibrations are visible in the IR, whereas at 20 h only broad, featureless IR bands are observed and at 80 h at 600 °C no bands pertaining to specific functional groups are visible (Fig. S6†). Therefore, thermal degradation at 600 °C is a very rapid process yielding highly porous, yet disordered nitrogen containing carbon materials.

3.4. Metal doping

The functionality of the *bipy* CTFs is largely determined by their high nitrogen content and in the samples synthesized at 400 °C by the molecularly well defined metal adsorption sites of the *bipy* linker. The interplay between the high surface area and micropore volume, and the resulting high density of metal coordination sites were probed by impregnating the framework with a solution containing an excess (fivefold with respect to the monomer providing one coordination site) of metal salt and monitoring the amount of metal taken up by the framework as well as its distribution in the material.

To this end, two *bipy* CTFs (*bipy* CTF 400 and *bipy* CTF 500) dispersed in water were exposed to different metal chlorides (K_2PtCl_4, $Na_2PdCl_4 \cdot 3H_2O$, $CoCl_2 \cdot 6H_2O$, and $NiCl_2 \cdot 6H_2O$) and the suspension was stirred at 60 °C overnight. After filtration and washing, the metal content adsorbed by the framework was determined by ICP analysis, and the uniformity of metal distribution in the framework was ascertained by EDX analysis as shown in Fig. S7†. The two CTF materials were selected in order to probe how the metal uptake varies as a function of synthesis temperature and, hence, porosity as well as nitrogen content and the resulting amount of specific bipyridine coordination sites.

As outlined in Fig. 8a and Table S4†, the highest metal uptake (in wt%) was observed for Pt, followed by Pd, Ni and Co. In general, the uptake by *bipy* CTF 500 increases by a factor of 1.5 to 3 compared to the uptake by *bipy* CTF 400, as *bipy* CTF 500 exhibits larger porosity and hence, accessibility of the coordination sites. The uptake of the heavier transition metal salts is generally larger than that of the lighter ones. The Pt and Pd uptake as a function of *bipy* CTF synthesis temperature shows a maximum for *bipy* CTF 500 and decreases towards higher synthesis temperatures (Fig. 8b and c). The NMR and IR results suggest that while in *bipy* CTF 500 the triazine nitrogen content is already essentially zero, there are still most of the *bipy*

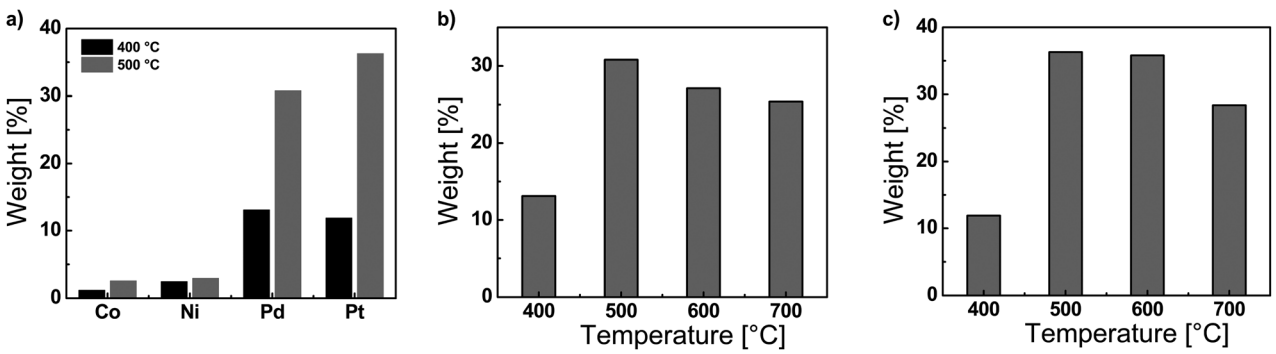

Fig. 8 (a) Metal uptake by *bipy* CTF 400 (black) and *bipy* CTF 500 (gray) in wt%. (b) Palladium and (c) platinum uptake by *bipy* CTFs synthesized at different temperatures.

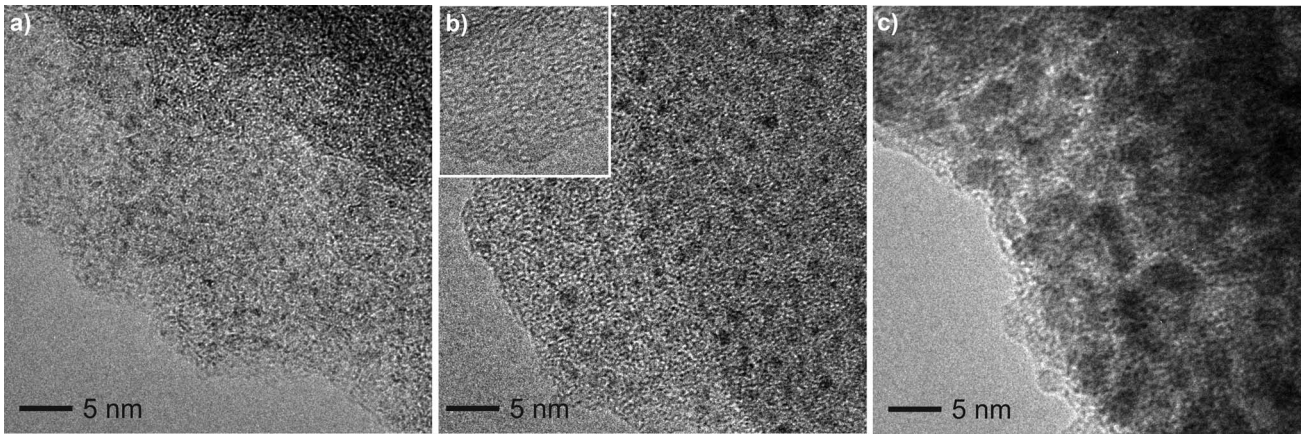

Fig. 9 TEM pictures of (a) Pt loaded and (b) Pd loaded samples (the inset shows an unloaded spot). (c) Pd nanoparticles in a Pd loaded sample.

coordination sites available. TEM and EDX data of the Pt and Pd samples show a uniform dispersion of the metals throughout the CTF (Fig. 9a and b). The atomic ratio of Pt and Cl is close to the theoretical one (1 : 2), indicating a coordination of $PtCl_2$ to the available *bipy* units (Fig. S7†). Remarkably, a small amount of Pt^0 and Pd^0 nanoparticles are also visible in the TEM (Fig. 9c), which is in agreement with the findings of Palkovits *et al.*[18] Note that the total amount of Pd^0 found in the samples is significantly higher than that of Pt^0. In both cases, however, the amount of metal formed is too small to be seen by XRD. In accordance with these results, the Pt and Pd uptake is governed by two counter acting trends the increase in surface area towards higher temperatures leads to increasing Pt and Pd uptake, while the concomitant decrease of available metal coordination sites by depletion of nitrogen leads to reduced Pt and Pd uptake. As a consequence, the maximum Pt and Pd uptake for *bipy* CTF 500 can be taken as indirect evidence of the *bipy* specific binding of Pt^{2+} and Pd^{2+}.

4. Conclusions

The presented *bipy* functionalized CTF lends itself as a model system to study the effects of different synthesis parameters on the structural and chemical properties of the obtained frame works. We have demonstrated a significant degree of tunability of the surface area and porosity as a function of temperature, resulting in hierarchically micro and mesoporous frameworks with high sorption capacity for various metal ions. The frame works show variable metal uptake, depending on the type of metal as well as the temperature at which the adsorbent was synthesized. Notably, enhanced Pt and Pd uptake at 500 600 °C suggests a rather specific Pt and Pd binding rather than mere dispersion of the metal on the CTF substrate. This type of binding ensures a "homogeneous" environment of the metal ions in the framework, which is highly robust and insoluble in essentially all organic solvents and strong acids. This finding bodes well for the use of metal modified *bipy* CTFs with high specific surface areas and high nitrogen content as heterogeneous catalysts with well defined metal coordination sites. Studies exploring the metal CTF interaction as well as the catalytic activity of metal doped *bipy* CTFs are currently underway.

Acknowledgements

We acknowledge support by the German Excellence Initiative of the Deutsche Forschungsgemeinschaft (DFG) *via* the Nano systems Initiative Munich (NIM), the Center for Nanoscience (CeNS) and the Fonds der Chemischen Industrie (FCI). M.E.T. thanks the Dr Alexander und Dr Rosemarie Bauer Stiftung for kind financial support. We thank Viola Duppel for TEM and SEM measurements, Christian Minke for SEM and ssNMR measurements, Andreas Wisnet, Teresa Dennenwaldt and Prof. Christina Scheu for TEM measurements, and Marie Luise Schreiber and Helmut Hartl for ICP AES measurements. We thank Mario Liebl and Prof. Jürgen Senker for providing us with the ^{15}N solid state NMR spectrum of CTF 1, and Prof. Thomas Bein, Prof. Wolfgang Schnick, and Prof. Wintterlin for access to the respective measurement facilities.

Notes and references

1 A. P. Côté, A. I. Benin, N. W. Ockwig, M. O'Keeffe, A. J. Matzger and O. M. Yaghi, *Science*, 2005, **310**, 1166 1170.
2 P. Kuhn, M. Antonietti and A. Thomas, *Angew. Chem., Int. Ed.*, 2008, **47**, 3450 3453.
3 J. L. C. Rowsell and O. M. Yaghi, *Microporous Mesoporous Mater.*, 2004, **73**, 3 14.
4 J. X. Jiang, F. Su, A. Trewin, C. D. Wood, N. L. Campbell, H. Niu, C. Dickinson, A. Y. Ganin, M. J. Rosseinsky, Y. Z. Khimyak and A. I. Cooper, *Angew. Chem., Int. Ed.*, 2008, **47**, 1167.
5 J. Y. Lee, C. D. Wood, D. Bradshaw, M. J. Rosseinsky and A. I. Cooper, *Chem. Commun.*, 2006, 2670 2672.
6 M. P. Tsyurupa and V. A. Davankov, *React. Funct. Polym.*, 2006, **66**, 768 779.
7 C. D. Wood, B. Tan, A. Trewin, H. Niu, D. Bradshaw, M. J. Rosseinsky, Y. Z. Khimyak, N. L. Campbell, R. Kirk, E. Stockel and A. I. Cooper, *Chem. Mater.*, 2007, **19**, 2034 2048.
8 P. M. Budd, B. S. Ghanem, S. Makhseed, N. B. McKeown, K. J. Msayib and C. E. Tattershall, *Chem. Commun.*, 2004, 230 231.
9 N. B. McKeown, P. M. Budd, K. J. Msayib, B. S. Ghanem, H. J. Kingston, C. E. Tattershall, S. Makhseed, K. J. Reynolds and D. Fritsch, *Chem. Eur. J.*, 2005, **11**, 2610 2620.
10 N. B. McKeown, B. Gahnem, K. J. Msayib, P. M. Budd, C. E. Tattershall, K. Mahmood, S. Tan, D. Book, H. W. Langmi and A. Walton, *Angew. Chem., Int. Ed.*, 2006, **45**, 1804 1807.
11 A. P. Côté, H. M. El Kaderi, H. Furukawa, J. R. Hunt and O. M. Yaghi, *J. Am. Chem. Soc.*, 2007, **129**, 12914 12915.
12 R. W. Tilford, W. R. Gemmill, H. C. zur Loye and J. J. Lavigne, *Chem. Mater.*, 2006, **18**, 5296 5301.

13 S. Wan, J. Guo, J. Kim, H. Ihee and D. Jiang, *Angew. Chem., Int. Ed.*, 2008, **47**, 8826 8830.
14 P. Kuhn, A. Thomas and M. Antonietti, *Macromolecules*, 2009, **42**, 319 326.
15 M. J. Bojdys, J. Jeromenok, A. Thomas and M. Antonietti, *Adv. Mater.*, 2010, **22**, 2202 2205.
16 C. E. Chan Thaw, A. Villa, P. Katekomol, D. Su, A. Thomas and L. Prati, *Nano Lett.*, 2010, **10**, 537 541.
17 C. E. Chan Thaw, A. Villa, L. Prati and A. Thomas, *Chem. Eur. J.*, 2011, **17**, 1052 1057.
18 R. Palkovits, M. Antonietti, P. Kuhn, A. Thomas and F. Schuth, *Angew. Chem., Int. Ed.*, 2009, **48**, 6909 6912.
19 A. Villa, D. Wang, P. Spontoni, R. Arrigo, D. Su and L. Prati, *Catal. Today*, 2010, **157**, 89 93.
20 K. Jiang, A. Eitan, L. S. Schadler, P. M. Ajayan, R. W. Siegel, N. Grobert, M. Mayne, M. Reyes Reyes, H. Terrones and M. Terrones, *Nano Lett.*, 2003, **3**, 275 277.
21 X. Hou, L. Wang, F. Zhou and F. Wang, *Carbon*, 2009, **47**, 1209 1213.
22 H. Yoon, S. Ko and J. Jang, *Chem. Commun.*, 2007, 1468 1470.
23 R. A. Periana, D. J. Taube, S. Gamble, H. Taube, T. Satoh and H. Fujii, *Science*, 1998, **280**, 560 564.
24 F. Tellier, R. Sauvêtre and J. F. Normant, *J. Organomet. Chem.*, 1985, **292**, 19 28.
25 D. W. Allen, B. G. Hutley and M. T. J. Mellor, *J. Chem. Soc., Perkin Trans. 2*, 1972, 63 67.
26 A. Krasovskiy and P. Knochel, *Synthesis*, 2006, 0890 0891.
27 F. M. Romero and R. Ziessel, *Tetrahedron Lett.*, 1995, **36**, 6471 6474.
28 P. N. W. Baxter and J. A. Connor, *J. Organomet. Chem.*, 1988, **355**, 193 196.
29 P. Kuhn, Al. Forget, D. Su, A. Thomas and M. Antonietti, *J. Am. Chem. Soc.*, 2008, **130**, 13333 13337.
30 V. G. Manecke and D. Wohrle, *Makromol. Chem.*, 1968, **120**, 176 191.
31 W. M. Padgett and W. F. Hamner, *J. Am. Chem. Soc.*, 1958, **80**, 803 808.
32 N. Neto, M. Muniz Miranda, L. Angeloni and E. Castellucci, *Spectrochim. Acta, Part A*, 1983, **39**, 97 106.
33 B. Jurgens, E. Irran, J. Senker, P. Kroll, H. Muller and W. Schnick, *J. Am. Chem. Soc.*, 2003, **125**, 10288 10300.
34 L. Pazderski, J. Toušek, J. Sitkowski, L. Kozerski and E. Szłyk, *Magn. Reson. Chem.*, 2007, **45**, 1045 1058.

